3-16-2022

Skip Nav Destination RESEARCH ARTICLE| MARCH 16, 2022 Assessing the effect of melt extraction from mushy reservoirs on compositions of granitoids: From a global database to a single batholith

J. Cornet
ETH Zürich

O. Bachmann
ETH Zürich

J. Ganne
University of Toulouse

A. Fiedrich
ETH Zürich

C. Huber
Brown University

See next page for additional authors

Authors

J. Cornet, O. Bachmann, J. Ganne, A. Fiedrich, C. Huber, C. D. Deering, and X. Feng

GOLD
OPEN ACCESS

THE GEOLOGICAL SOCIETY OF AMERICA®

Assessing the effect of melt extraction from mushy reservoirs on compositions of granitoids: From a global database to a single batholith

J. Cornet[1], O. Bachmann[1], J. Ganne[2], A. Fiedrich[1], C. Huber[3], C.D. Deering[4], and X. Feng[5]

[1]ETH Zürich, Department of Earth Sciences, Clausiusstrasse 25, 8092 Zürich, Switzerland
[2]Géosciences Environnement Toulouse (GET), French National Research Institute for Sustainable Development, French National Centre for Scientific Research (CNRS), University of Toulouse, Toulouse 31400, France
[3]Department of Earth, Environmental and Planetary Sciences, Brown University, 324 Brook Street, Providence, Rhode Island 02912, USA
[4]Department of Geological and Mining Engineering and Sciences, 630 Dow Environmental Sciences, Michigan Technological University, 1400 Townsend Drive, Houghton, Michigan 49931, USA
[5]School of Safety Engineering, China University of Mining and Technology, Jiangsu 221116, China

ABSTRACT

Mafic and ultramafic plutonic rocks are often considered to be crystal cumulates (i.e., they are melt-depleted), but such a classification is much more contentious for intermediate to silicic granitoids (e.g., tonalite, granodiorite, granite, and syenite). Whether or not a given plutonic rock has lost melt to feed shallower subvolcanic intrusive bodies or volcanic edifices has key implications for understanding igneous processes occurring within the crust throughout the evolution of the Earth. We use statistical analyses of a global volcanic and plutonic rock database to show that most mafic to felsic plutonic rock compositions can be interpreted as melt-depleted (i.e., most of the minerals analyzed are more evolved than their bulk-rock compositions would allow). To illustrate the application of the method to natural samples (from the Tertiary Adamello Batholith in the southern Alps), we estimate the degree of melt depletion using a combination of magmatic textures, bulk-rock chemistry, modal mineralogy, distributions of plagioclase composition (using scanning electron microscope phase mapping/electron microprobe analyses), and thermodynamic modeling. We find that melt depletion correlates with the magmatic foliation and is accompanied by bulk depletion in incompatible elements, low amounts of near-solidus minerals, and mineral compositions that are too evolved (i.e., depleted in Ca or Mg, depending on the mineral) to be in equilibrium with their bulk-rock chemistry. The analytical and modeling workflow proposed in this study provides a path to quantifying melt depletion in any plutonic samples.

> Most plutons cannot be assumed to represent liquids; degree of crystal-liquid separation must be a major consideration in their interpretation, whether or not cumulate textures are obvious. (Bacon and Druitt, 1988, p. 253)

> Igneous rocks, especially plutonic rocks, rarely represent quenched melts. (Miller et al., 2003, p. 529)

■ INTRODUCTION

The understanding that plutonic rocks can represent crystal accumulation zones and deviate significantly from liquid lines of descent has been accepted for decades, particularly for mafic rocks (Arculus and Wills, 1980; Barnes et al., 2016; Berger et al., 2017; Boudreau and Philpotts, 2002; Jagoutz and Schmidt, 2012; Lewis, 1973; Meurer and Boudreau, 1996; Putirka, 2017; Shirley, 1986; Wager et al., 1960; Wager, 1962). Whether or not intermediate to silicic mushy reservoirs can lose significant amounts of interstitial melt (and turn into intermediate to silicic cumulates), however, remains a topic of debate (Bachl et al., 2001; Bachmann and Huber, 2019; Barnes et al., 2016; Beane and Wiebe, 2012; Bertolett et al., 2019; Deering and Bachmann, 2010;

Frazer et al., 2014; Garibaldi et al., 2018; Gelman et al., 2014; Graeter et al., 2015; Hartung et al., 2017; Keller et al., 2015; Lee and Morton, 2015; Memeti et al., 2010; Putirka et al., 2014; Tappa et al., 2011; Walker et al., 2015; Wiebe and Collins, 1998; Wolff, 2017). For instance, many intermediate to silicic plutonic rocks were used to frame liquid lines of descent in magmatic provinces of all ages (Bigazzi et al., 1986; Bogaerts et al., 2003; Chappell et al., 1988; Duchesne et al., 1998; Frey et al., 1978; Glazner et al., 2018; Hoskin et al., 2000; Moyen et al., 2001; Perfit et al., 1980; Stephens et al., 1985; Wyborn et al., 2001). However, if some of the plutonic samples analyzed underwent a physical separation of melt and crystals during their supra-solidus lifetimes, the bulk-rock composition required to characterize liquid lines of descent, depth of melt generation, or even a tectonic setting, could lead to severely biased interpretations. Hence, finding ways to test whether a given plutonic rock lost melt (and potentially quantify the amount of melt loss) is fundamental to research focusing on crustal growth and evolution. It would also allow a better characterization of the volcanic/plutonic ratio in a given magmatic province, which is a key, albeit elusive, parameter in understanding secondary crustal formation and growth on rocky planets (Taylor, 1989).

In this study, we use the GEOROC geochemical database to determine which, if any, plutonic rocks are cumulative in nature, particularly those with a magmatic fabric (e.g., foliation) and intermediate compositions (e.g., granodiorite, tonalite,

Julien Cornet https://orcid.org/0000-0002-6517-5456

and syenite). However, samples from this large database typically lack petrographic/petrologic context and, therefore, present a challenge for determining the exact processes involved in generating the observed geochemical trends. Hence, to complement our statistical analysis of the GEOROC database, we consider a suite of samples from the well-studied Adamello Batholith (Tertiary Alpine Batholith in the southern Alps; Hansmann and Oberli, 1991; Kagami et al., 1991; Schoene et al., 2012, Fiedrich et al., 2017) for which we have clear geochemical, petrological, and textural context.

Our analysis of samples from the Adamello Batholith follows a workflow based on a comprehensive analytical and thermodynamic modeling effort. Specifically, we compare the actual distribution of plagioclase anorthite (An) content in a given sample (determined through analysis of secondary electron microscope [SEM] chemical maps coupled with electron microprobe [EMP] analyses) to the modeled "ideal" distribution based on closed-system thermodynamics. This strategy can be combined with methods for determining the extent of melt loss in plutons that preserve their magmatic textures and compositions (Bertolett et al., 2019; Fiedrich et al., 2017; Garibaldi et al., 2018; Webber et al., 2015) by quantifying the amount of trapped melt and the fabric strength. It can also be compared with other geochemical methods developed to quantify melt loss in granitic systems (Deering and Bachmann, 2010; Gelman et al., 2014; Werts et al., 2020; Barnes et al., 2020).

■ METHODS

Statistics on the Global Plutonic Database

We use a compilation of igneous data from GEOROC (http://georoc.mpch-mainz.gwdg.de/georoc/) in which the bulk-rock composition and associated mineral analyses were matched by Ganne et al. (2018); see Supplemental Material File S1[1]. Our data are filtered to exclude all rock samples with major oxide totals outside a 95–101.5% range, assuming they underwent some type of alteration or were poorly analyzed. The GEOROC database contains fewer mineral analyses for plutonic rocks (n = 615) than volcanic rocks (n = 5958). Additionally, the database is biased toward gabbroic and granitic compositions, which means that intermediate compositions are underrepresented (Ganne et al., 2018). We used GEOROC to evaluate disequilibrium among minerals and their respective bulk rocks across a range of compositions (cf. hereafter "*Testing chemical equilibrium among bulk rocks and minerals*"). As such, we rely on a procedure based on Monte Carlo analyses with bootstrap resampling to mitigate the sampling bias (Keller et al., 2015). The procedure was conducted as follows: (1) a subset of data was randomly selected so that the probability of inclusion in the resampled subset was directly proportional to the sample weight (calculated as

$$sample\ weight =$$
$$\frac{Target\ proportion\ of\ the\ sample\ (\%)}{Observed\ proportion\ of\ the\ sample\ (\%)},$$

which ensures that less represented bulk-rock compositions are resampled more); (2) a synthetic data set for each sampled data point was drawn from a Gaussian distribution with a mean equal to the original value of the data point and the standard deviation equal to the estimated 1 standard uncertainty of the data point; (3) the resulting data were sorted into bins of composition (e.g., 1 bin = 1 SiO_2 wt% of rocks), with a mean and variance calculated for each variable; (4) steps 1–3 were repeated 1000 times. For statistical reasons, we set a minimum number of samples (threshold of three) within each bin to perform steps 1–3 and, therefore, yield a more robust evaluation of equilibrium; (5) a total mean and standard error of the mean were calculated for each variable (e.g., bootstrapped values) in each bin (e.g., range of compositions). The standard error $\sigma_{\bar{x}}$ of the sample mean (noted as: $\sigma_{\bar{x}} = \frac{\sigma}{\sqrt{n}}$, with σ the standard deviation and n the sample size) gives an estimate of how far our sample error may be from the true population mean. The population mean is within two times the standard error of the sample mean ~95% of the time. Our estimations of equilibrium are reported with 1 standard deviation of the sample mean at different intervals of bulk-rock composition (e.g., SiO_2 wt%).

Testing Chemical Equilibrium among Bulk Rocks and Minerals

Following the same approach as Ganne et al. (2018), which focused on the extent and nature of mineral disequilibrium within their host rock in *volcanic* systems, we herein concentrate our investigation on the *plutonic rocks* recorded in the GEOROC database. The database with the matched compositions for bulk plutonic rocks and associated minerals is available in File S1; see footnote 1.

We test for equilibrium among the minerals and a nominal, coexisting liquid by comparing observed and predicted Fe-Mg or An-Ab exchange values, or $KD^{Min/liq}_{Fe-Mg}$ and $KD^{Min/liq}_{Ca-Na}$ (Putirka, 2008, 2016), of minerals and their hosting bulk-rock compositions. $KD^{Min/liq}_{Fe-Mg}$ are 0.28 ± 0.11 for clinoamphibole, 0.27 ± 0.03 for clinopyroxene, 0.29 ± 0.06 for orthopyroxene, and 0.30 ± 0.03 for olivine. For plagioclase feldspars, the equilibrium constant depends on T (Putirka, 2008); at T < 1050 °C, the equilibrium constant is 0.1 ± 0.05, while for T > 1050 °C, it is 0.27 ± 0.11. If a mineral is in equilibrium with its bulk rock, the putative liquid mineral pair should lie within the equilibrium values (within the established uncertainty) given by the equilibrium constant. If out of equilibrium, the mineral compositions, relative to bulk-rock compositions, are either:
(1) less evolved, with more Ca in plagioclase or more Mg in mafic minerals, or
(2) more evolved, with less Ca in plagioclase or less Mg in mafic minerals.

To visualize the disequilibrium of the minerals and corresponding host rocks in our global data set, we used a modified representation of

[1]Supplemental Material. Includes database with matched compositions for bulk plutonic rocks and associated minerals; detailed tutorial for using iSpectra®; and more exhaustive set of simulations. Please visit **https://doi.org/10.1130/GEOS.S.19089920** to access the supplemental material, and contact editing@geosociety.org with any questions.

the Rhodes diagram (e.g., wt% instead of mol; Rhodes et al., 1979) and applied it specifically to plagioclase. We used the CaO/(CaO+Na$_2$O) ratio in the host plutonic rocks (i.e., which is supposed to represent the original melt composition) and plagioclase to test for equilibrium. The reasons for focusing on plagioclase are:

(1) Plagioclase is the dominant mineral in many intermediate to silicic plutonic rocks.

(2) Due to slow intracrystalline diffusion of the major elements in plagioclase, a rich record of the variations in melt composition (due to mixing, assimilation, and other magmatic processes), temperature, pressure (Putirka, 2008, and references therein), and dissolved water contents (i.e., hygrometer, Fiedrich et al., 2018; Waters and Lange, 2015) are typically preserved.

Hence, plagioclase is a reasonable choice as an archive for varying crystallization conditions in magma reservoirs.

We also report calculations from the volcanic record (from Ganne et al., 2018) to directly compare the extent and nature of potential disequilibrium among plagioclase in plutonic and volcanic rocks. Additionally, we evaluate the extent of disequilibrium of amphibole and clinopyroxene using a modified Rhodes diagram for plutonic and volcanic rocks (File S2; see footnote 1).

Analytical Workflow for Identifying Silicic Cumulates

Field and Analytical Methods for Tracking Silicic Cumulates

The workflow presented in this study starts with the selection of a non-altered plutonic rock sampled from a single batholithic suite with obvious field relationships and pristine magmatic fabrics and textures (e.g., no faults, no deformation, and no metamorphism). Bulk-rock composition and optical microscope/scanning electron microscope (SEM) observations of the samples are then required to constrain the: (1) compositional variability, (2) texture, (3) fabric, and (4) amount of modal variability among the different samples.

Once samples are identified, geochemical analyses from representative primary minerals are needed to assess the occurrence and extent of disequilibrium among the minerals and the bulk-rock compositions (i.e., how cumulative or how far from a liquid a given sample is). Presently, the existing techniques for assessing melt loss by comparing mineral and bulk-rock chemistries rely on using major and trace element contents of amphiboles and comparing them to their host-rock compositions. For instance, Werts et al. (2020) used the distribution coefficient of Fe-Mg between amphibole and melt to evaluate the extent of disequilibrium among amphiboles and their bulk rock, while Barnes et al. (2020) used estimates of zircon saturation given by major elements and Zr for bulk rock and amphiboles. As described below, we argue that plagioclase compositional histograms from high-resolution quantitative phase maps obtained by scanning electron microscopy (SEM; i.e., iSpectra®, Liebske, 2015) provides another powerful technique for assessing whether a given plutonic rock sample is a cumulate or not.

Phase Mapping

Phase mapping utilizes element maps via the SEM that are then processed using iSpectra®. The SEM elemental maps were generated using a Thermo Fisher Ultradry energy-dispersive X-ray spectroscope (EDS) coupled to a Thermo Fisher Noran system 7 mounted on a Jeol JSM-6390LA to scan representative areas of a 20 nm carbon-coated thin section at the Department of Earth Sciences at ETH Zurich. The LaB$_6$ filament was set with an acceleration voltage of 15kV to measure the spectra of all major elements. Scanmode of the SEM operated 128 × 96 pixel maps with 10 frames per 60 s, yielding ~22,700 counts per second. The element maps were processed using iSpectra® (Liebske, 2015), an add-on program of the software IGOR Pro®. A detailed tutorial for using iSpectra® is available in File S3 (see footnote 1). We assume that Area% can be used as a proxy for Volume%. The anorthite content of plagioclase is determined through a calibration line (Fig. 1) based on the net counts of Al/Si in the minerals implemented in iSpectra®. The calibration line is:
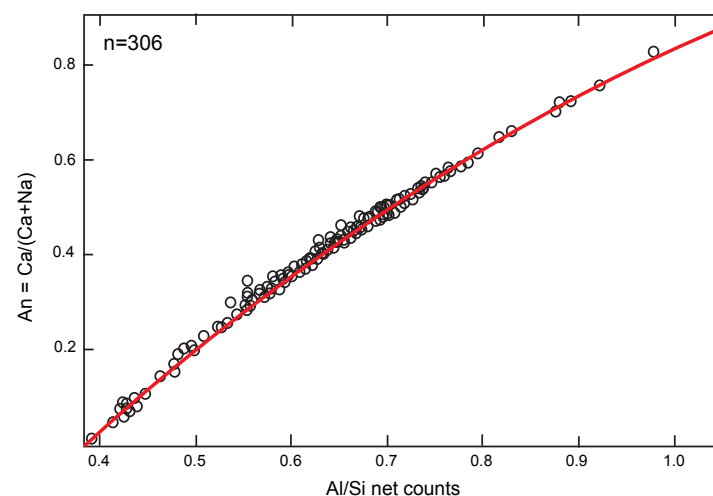

Figure 1. An versus Al/Si calibration line was obtained from energy-dispersive X-ray spectroscope (EDS) and electron microprobe (EMP) spot analyses of plagioclase from five samples of Adamello Batholith. Two external samples were used to extend the calibration line to very low anorthite contents and illustrate the applicability of the calibration line to samples of variable compositions.

Cornet et al. | Assessing the effect of melt extraction on compositions of granitoids

$$An = 1.68 - 1.67 * \exp\left(-\frac{\frac{Al}{Si} - 0.39}{0.91}\right) * 100.$$

This calibration line allows for a bin size resolution of 5 mol% for the An content. The calibration equation can be further refined by adding more EMP or EDS data of core to rim plagioclase traverses for a given set of plagioclase crystals within samples.

Thermodynamic Simulations

Once the distribution of plagioclase compositions is obtained for a given sample, it can be compared to a simulated distribution of plagioclase compositions obtained under closed-system conditions using thermodynamic simulations. The guiding principle here is that *if* the bulk composition of the plutonic sample represents a liquid composition, then thermodynamic calculations should reproduce the mineral compositions (within the current limitations of the thermodynamic models). Assessment of appropriate storage conditions of the magma (pressure, fO_2, and water content) is necessary to generate accurate modeled phase compositions through the stages of melt evolution. Typically, thermodynamic models such as rhyolite-MELTS (Gualda et al., 2012) or Perple_X (Connolly, 2009) use Gibbs free energy minimization to compute equilibrium compositions.

Thermodynamic Simulations Applied to the Plagioclase Population of Adamello Samples

We use the open source MELTS package provided online under the name xMELTS (https://gitlab.com/ENKI-portal/xMELTS) adapted to run in Matlab® on Linux and Mac operating systems. We call the script MatMELTS, which can be provided on request. This script is capable of running a large number of calculations in a short amount of time. Different MELTS versions can be named (i.e., rhyolite_MELTS v1.x.x, pMELTS) for the main calculation modes ("batch" for equilibrium crystallization, "fractionate solids" for fractional crystallization and

others) and for setting intensive (temperature, pressure) and extensive (composition, H_2O/CO_2 content, and oxygen fugacity) parameters.

We will show a series of thermodynamic simulations with the MatMELTS script (using rhyolite_MELTS version 1.2.x) where the initial conditions span different water contents (4 wt%, 5 wt%, and 6 wt%) at 2 kbar over a temperature range of 1100–700 °C using a fixed fo_2 buffer of FMQ +1 (for typical range of conditions for the Adamello rocks studied, see Marxer and Ulmer [2019]). Our goal is to compare the An distribution obtained with the SEM maps with outputs from simulations in *batch* and *fractionate solid* modes. Additionally, at crystallinities lower than 50 vol%, we assume that: (1) little to no phase separation occurs and (2) the system remains close to equilibrium. However, phase separation can occur as the rheological lock-up is reached (~50% of crystallinity; Vigneresse et al., 1996), and the system tends to depart from equilibrium. Therefore, we use a crystallinity threshold that switches from batch to fractional crystallization during the MatMELTs calculations. The switch takes the melt composition at a prescribed crystallinity from the *batch* simulations, which is then used as a starting composition for fractionation calculations. In this study, we use 40%, 50%, and 60% crystallinity ($F_{cryst} = 1 - F_{melt}$, 40/60, 50/50, 60/40) and record the composition of the plagioclase population along the liquid lines of descent. Some results are presented in the main text, and a more exhaustive set of simulations can be found in File S4 (see footnote 1).

■ RESULTS

Statistical Analysis of the GEOROC Database for Melt-Crystal Disequilibrium

For the plutonic rocks, the GEOROC database provides 5958 mineral analyses within 615 plutonic bulk-rock samples. The occurrence and extent of disequilibrium between each mineral analysis with its respective bulk-rock host is tested using the methods described earlier (cf., Methods section). The global statistical result of the equilibrium test for all kinds of minerals explored (Fig. 2) indicates

that 65% of the tabulated plutonic rocks in the database have over 90% of their respective mineral assemblages in disequilibrium. This result indicates that most of the plutonic rocks in the GEOROC database have either more evolved or less evolved minerals (see definitions in Testing Chemical Equilibrium between Bulk Rocks and Minerals section) than the host plutonic bulk-rock equilibrium compositions.

Most minerals in volcanic systems are expected to have crystallized near equilibrium with the bulk-rock compositions (i.e., assuming most are "phenocrysts"). Therefore, we use the above-mentioned method to test for equilibrium among volcanic rocks and associated minerals from GEOROC. The results are presented as a boot-strapped evaluation of equilibrium for ol, amph, opx, pl, and cpx against the silica content of the host bulk rocks that aid in determining an "Average Equilibrium" (AE) useful for assessing the proportions of minerals in equilibrium with their bulk rocks from mafic to silicic compositions (Fig. 3). In the case of plagioclase (i.e., the most represented mineral across the whole range of bulk-rock compositions), the "average equilibrium" is low for plutonic rocks (AE = 22%) and significantly higher for volcanic rocks (AE = 48%). Similarly, the amphibole record also demonstrates that disequilibrium is more pronounced in the plutonic record. Although less representative in sample size and/or occurrence in all bulk-rock compositions (e.g., SiO_2 wt% of bulk rock), all other minerals (cpx, opx, and olivine) support this interpretation (see Files S1–S2).

The comparison of volcanic and plutonic rocks indicates that plutonic minerals statistically show more disequilibrium with their associated bulk rocks than volcanic minerals do. When evaluating the *nature* of disequilibrium among minerals and bulk-rock pairs (i.e., checking if minerals are more- or less-evolved than their bulk-rock compositions), we are able to recognize another major difference between the volcanic and plutonic data sets (Fig. 4). Our statistical evaluation of minerals (e.g., amph, ol, opx, cpx, and pl) characterized by a *less evolved composition than their bulk rocks* (i.e., more Ca-rich for plagioclase, more Mg-rich for the Fe-Mg phases) reveals that few plutonic minerals are, in fact, less

Cornet et al. | Assessing the effect of melt extraction on compositions of granitoids
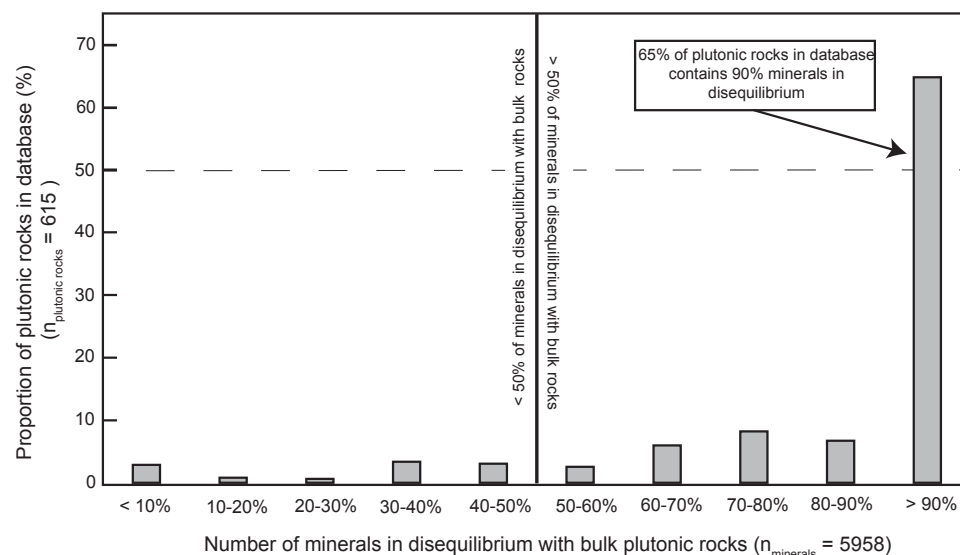
Figure 2. Frequency of disequilibrium among minerals (olivine, amphibole, orthopyroxene, clinopyroxene, and plagioclase) and their host plutonic rocks in the GEOROC database is shown.

evolved than the bulk-rock composition of the sample from which they are derived (Fig. 4, yellow bars, only ~6% of the minerals). In contrast, using the same test for the volcanic data shows a higher proportion of minerals that are less evolved than their host bulk-rock composition (average of ~36% of the volcanic mineral assemblage). These statistics indicate that most of the plutonic mineral assemblage is biased toward a *more evolved* composition than its bulk-rock composition would suggest.

Evaluation of the Equilibrium among the GEOROC Plagioclase Population and Bulk Plutonic and Volcanic Compositions

We evaluate the discrepancies between volcanic and plutonic data by using a modified version of Rhodes diagrams for the plutonic and volcanic plagioclase–bulk rock (considered to be initial melt compositions) pairs in the GEOROC database using the $KD_{Ca-Na}^{Min/Liq}$ of plagioclase and bulk rocks (Fig. 5).

These diagrams reveal the amount of mineral disequilibrium as well as the magnitude and direction of disequilibrium of each data point. When combined into bootstrapped equilibrium values (red points in Fig. 5) for each range of bulk-rock compositions [e.g., CaO/(CaO +Na$_2$O)], an equilibrium line can be drawn for the entire range of bulk-rock compositions for the plutonic and volcanic mineral host pairs. Similarly, bootstrapped disequilibrium values (black points in Fig. 5) display the variations of magnitude and direction of disequilibrium in the entire range of bulk-rock compositions in both systems from which a disequilibrium line can be drawn. The main observation is that the plutonic plagioclase population obtained with bootstrapping is more evolved relative to the equilibrium curve whereas, for the volcanic database, the plagioclase population encompasses both more and less evolved compositions relative to the equilibrium curve (Fig. 5). These observations highlight that there are major differences between the plutonic and volcanic mineral assemblages in

terms of amount and direction of disequilibrium along a wide range of bulk-rock compositions.

The magnitude and direction of disequilibrium between minerals and the host bulk-rock compositions suggest an important influence from open-system processes. In the case of the volcanic compositions in the database, the less evolved nature of the mineral assemblage of the intermediate rock compositions (e.g., andesites/dacites) suggests frequent primitive recharge, which leads to mixing and mingling among different batches of magma (Fig. 5; Ganne et al., 2018). In the case of the plutonic compositions in the database, the more evolved nature of the mineral assemblage of all bulk-rock compositions suggests that some melt loss may have fed shallower systems (hypabyssal intrusions, porphyries, and/or volcanic units) or remained close to the host magma source. Alternatively, the more evolved nature of the minerals can also be partly explained by melt evolution under closed-system conditions (leading to normal zoning and evolved rims on the minerals). However, if a closed system dominates, the initial bulk-rock composition at the origin of a plagioclase population would be preserved. For an open system, melt depletion at some instance during the life of a magma changes the bulk-rock composition and inhibits the preservation of the initial bulk composition (see annotated diagram for the plutonic database in Fig. 5).

Our statistical investigation using GEOROC shows that the volcanic and plutonic rock/mineral compositions have fundamental differences in terms of equilibrium/disequilibrium and indicates that plutonic rocks may, indeed, be mainly affected by melt extraction mechanisms. However, the lack of a petrological context for each sample in these databases precludes a detailed analysis of how much melt a given sample might have lost. Therefore, one needs additional constraints that can only be obtained by thoroughly analyzing individual plutonic samples in a given geological setting. Hereafter, we use samples from the Adamello Batholith to test these disequilibrium characteristics observed in the database of plutonic bulk and mineral compositions. A previous study of the textural fabrics and compositions of these

Cornet et al. | Assessing the effect of melt extraction on compositions of granitoids
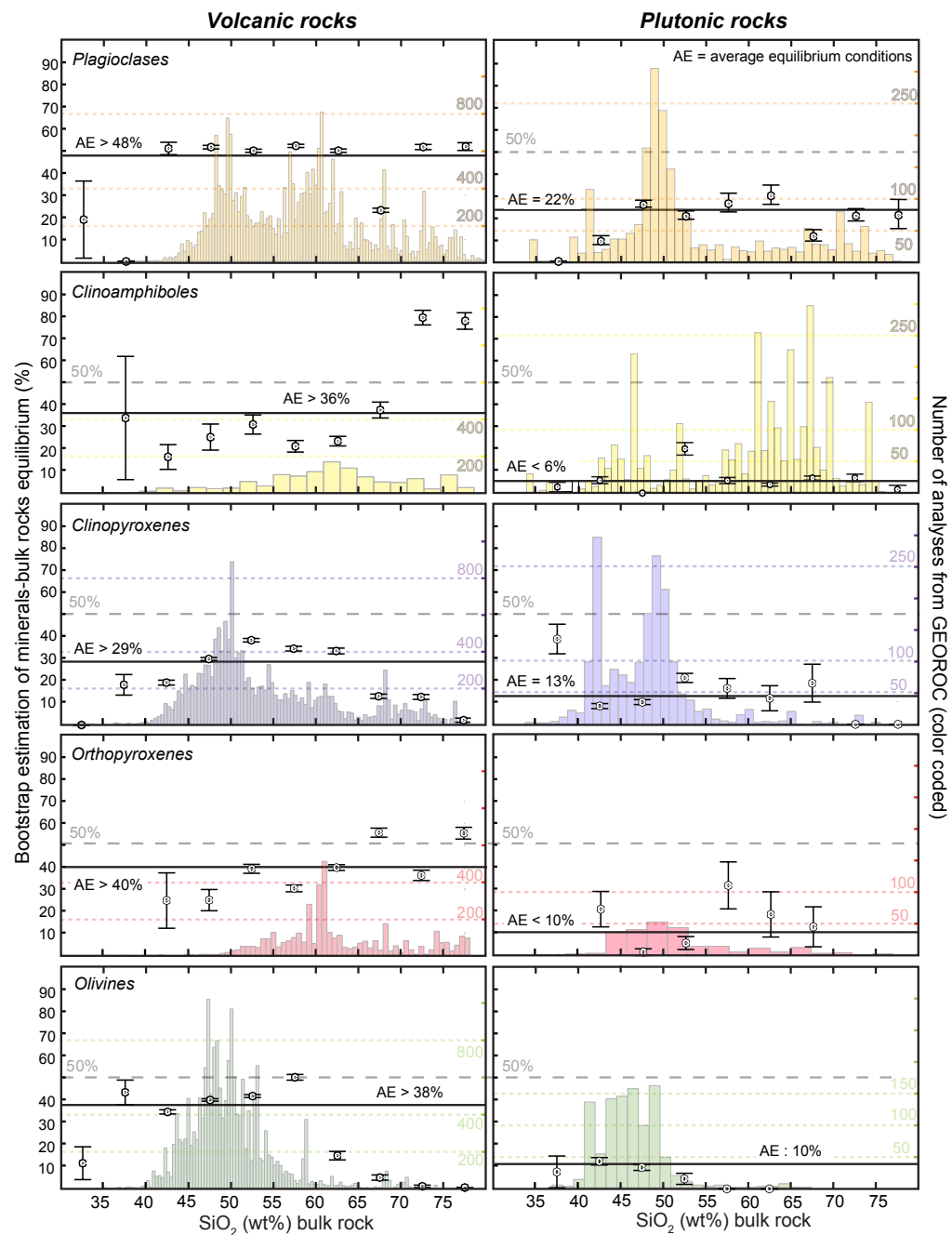
Figure 3. Results of the bootstrap analyses of volcanic and plutonic rocks give the percentage of minerals in equilibrium with their respective bulk rocks. The bootstrap analyses were calculated every increment of 5 wt% SiO_2 and are shown with ± 1σ (see text). Colored histograms in the background show the number of available analyses in the database for each mineral binned according to the bulk SiO_2 content. The bin size varies according to the number of analyses available.
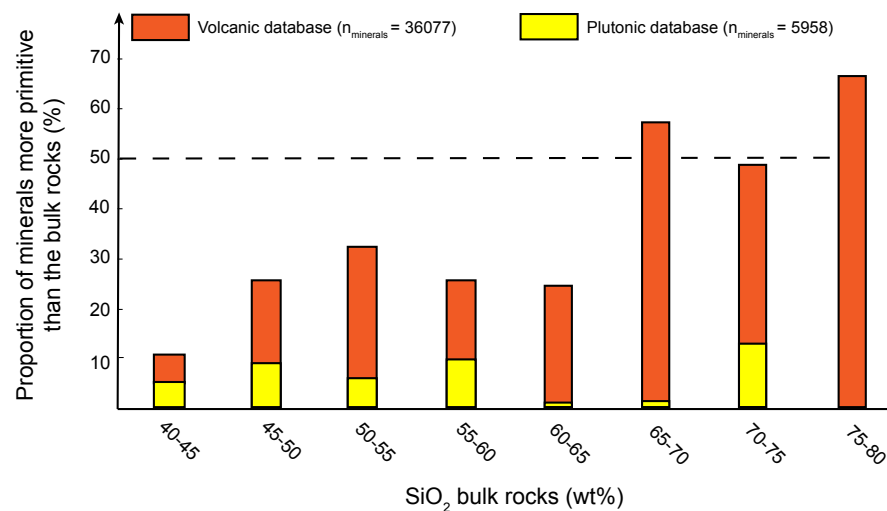
Figure 4. Percentage of crystalline phases (olivine, clinopyroxene, orthopyroxene, plagioclase, and amphibole) that are less evolved than their bulk volcanic rocks (orange bars) and plutonic rocks (yellow bars). See definition of "less evolved" in the text. Here, crystals in equilibrium are not considered, and data are plotted against the range of magma composition (SiO_2 wt%) hosting the mineral assemblages. The dashed line is a reference line at 50% for visual purposes.

TABLE 1. BULK-ROCK GEOCHEMICAL DATA AND ESTIMATED TRAPPED LIQUID FOR THE TWO ENDMEMBER SAMPLES AV1A AND AF15, REPORTED FROM FIEDRICH ET AL. (2017)

Sample	AV 1a	AF 15
Major elements (wt%)		
SiO_2	53.63	63.89
TiO_2	0.86	0.52
Al_2O_3	19.45	17.01
Fe_2O_3	8.16	4.92
MnO	0.22	0.11
MgO	3.05	2.13
CaO	9.18	5.74
Na_2O	3.95	3.03
K_2O	0.74	2.10
$P2O_5$	0.30	0.16
Total	99.98	100.24
Trace elements (ppm)		
Rb	11.81	77.97
Cs	0.15	3.40
Sr	512.66	379.72
Ba	233.14	581.31
Zr	69.68	122.26
Hf	1.99	3.11
Nb	7.28	12.96
Ta	0.35	1.09
Y	21.71	16.82
La	21.99	47.64
Ce	42.85	81.94
Pr	5.19	8.18
Nd	21.03	27.27
Sm	4.37	4.54
Eu	1.45	1.02
Gd	4.22	3.50
Tb	0.62	0.52
Dy	4.02	2.91
Ho	0.85	0.56
Er	2.24	1.65
Tm	0.28	0.24
Yb	2.56	1.82
Lu	0.36	0.28
Pb	4.05	12.00
Th	4.77	19.30
U	0.99	3.73
Estimated amount of trapped liquid (%)		
Minimum	7	29
Maximum	31	62

samples provides additional constraints that permit quantitative estimates of melt loss (Fiedrich et al., 2017; Table 1). We use this case study to illustrate the benefit of applying the proposed workflow to individual plutons around the world.

Recognizing and Characterizing Silicic Cumulates: Insights from the Adamello Batholith

The Adamello Batholith in northern Italy formed as a consequence of Alpine magmatism that intruded a Permo-Mesozoic sedimentary cover between 43 Ma and 31 Ma (Schaltegger et al., 2009). This batholith exposes typical calc-alkaline, metaluminous rocks, from gabbros to granodiorites, emplaced mostly in the upper crust (between 2 kbar and 3 kbar; Pennacchioni et al., 2006). The samples selected for use in this study come from two main units: Re Di Castello (RdC) and the Western Adamello Tonalites (WAT).

We chose two end members of our Adamello sample collection (AV1a from RdC and AF15 from WAT) based on their distinct texture, fabric, mode, and composition (Table 1, Fig. 6A.i and Fig. 6B.i). Such differences were described in detail by Fiedrich et al. (2017). AV1a is a quartz diorite with ~54 wt% SiO_2, while AF15 is a granodiorite (close to the tonalite field) with ~64 wt% SiO_2. AV1a is the sample with the lowest proportion of trapped melt, which ranges from a minimum of ~7% to a maximum of ~30%, and AF15 has the highest proportion of trapped melt, ranging from a minimum of ~30% to a maximum of ~60% (Table 1; Fiedrich et al., 2017). The samples have identical mineral assemblages, but the modes vary significantly between the two samples as do elemental concentrations. Modes display low K-feldspar amounts (much lower than those of any potential haplogranitic melts; Fig. 7A; Johannes and Holtz, 1996; Tavazzani et al., 2020; Tuttle and Bowen, 1958), in particular for AV1a. Similarly, elements compatible with the observed mineral assemblage (plagioclase, amphibole, Fe-Ti oxides, and apatite) are enriched in AV1a, whereas typically incompatible elements (e.g., K, Rb, Ba, and LREE) are more abundant in AF15 (Fig. 7B). AV1a
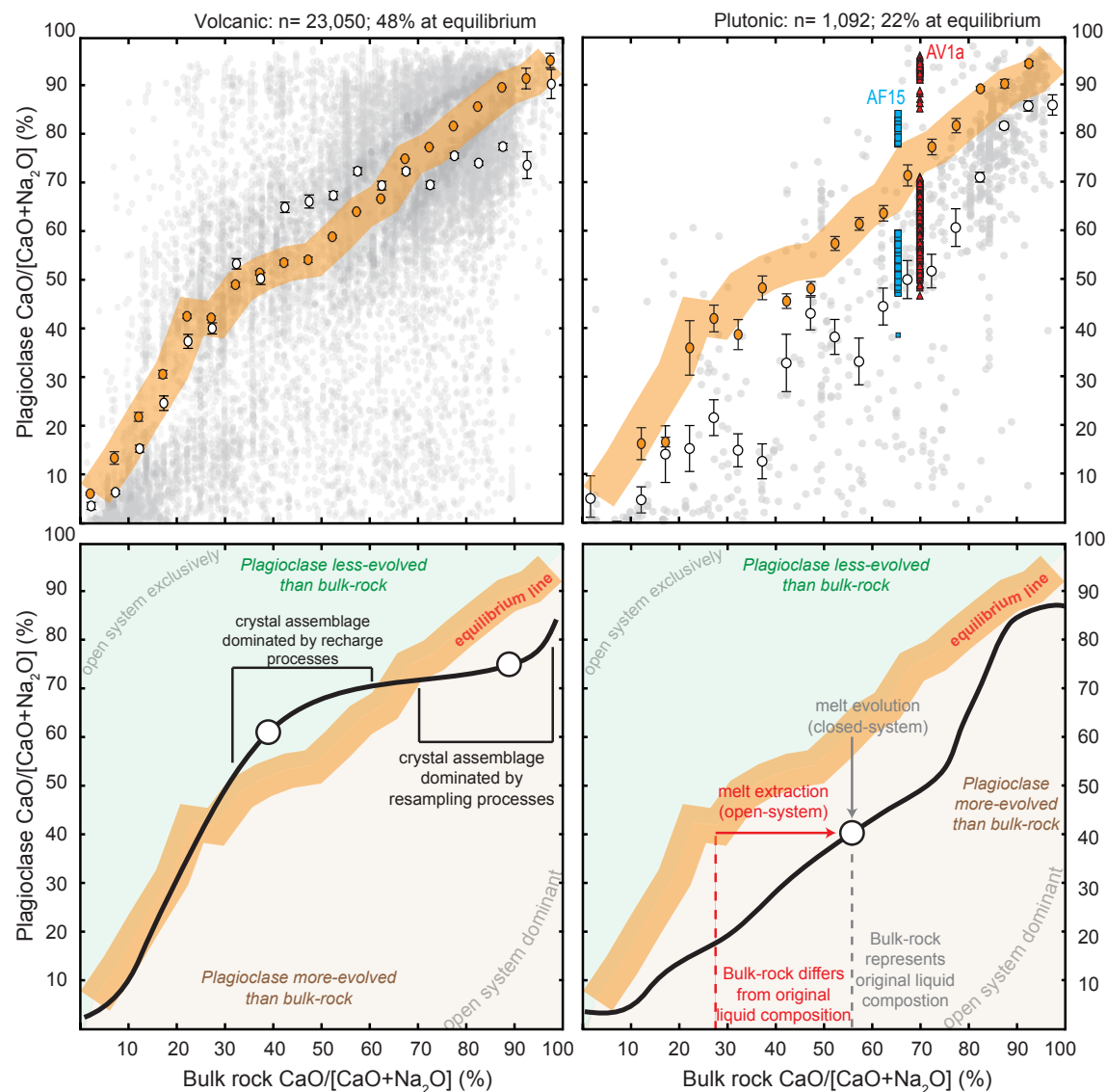
Figure 5. Bootstrapped tests for equilibrium (orange and white circles) obtained from plagioclase crystals and their associated volcanic and plutonic bulk rocks (gray circles) are plotted. The orange bootstrapped values fall into the equilibrium range, and white bootstrapped values imply disequilibrium. Bootstrap analyses are calculated for each increment of five of the CaO/[CaO + Na$_2$O] of the bulk-rock composition, and the uncertainty bars correspond to ± 1σ from mineral analyses. The range of plagioclase in disequilibrium from the Adamello Batholith samples is showed in blue (AF15) and red (AV1a) on the plutonic rock panel. The bootstrapped tests for equilibrium for the volcanic and plutonic databases are summarized to equilibrium and disequilibrium lines and annotated to clarify the information given by the modified versions of Rhodes diagrams using wt% of oxides.
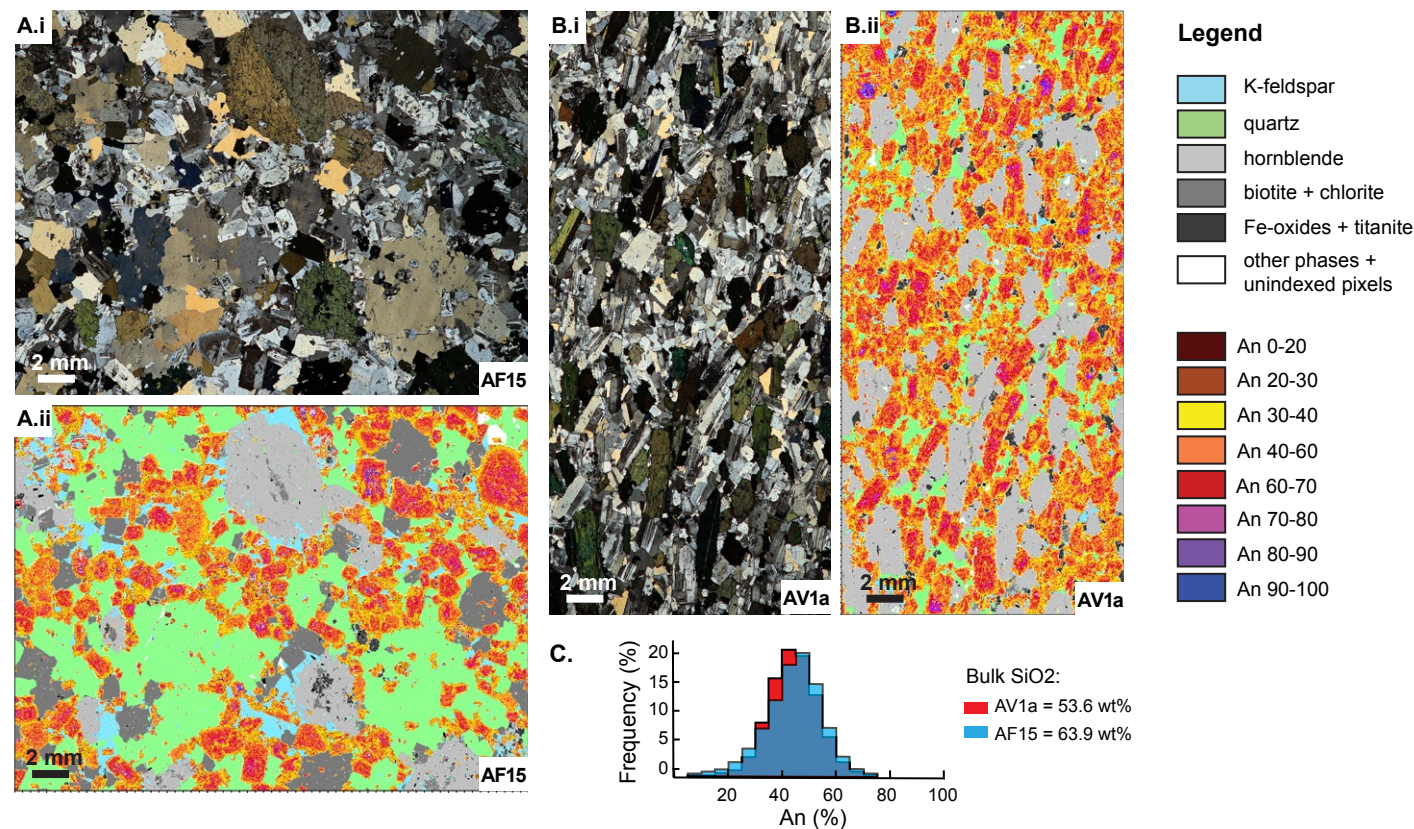
Figure 6. Crossed-polar photomicrographs and phase maps obtained by scanning electron microscope mapping are shown for AV1a and AF15 (including plagioclase compositions binned by 10% Anorthite). (A.i) Crossed-polar photomicrograph of AF15. (A.ii) An map of AF15. (B.i) Crossed-polar photomicrograph of AV1a. (B.ii) An map of AV1a. (C) Frequency histogram of the An population of AV1a and AF15 from the An maps.

also displays a stronger magmatic fabric than AF15 (Fig. 6A.i and Fig. 6B.i; Fiedrich et al., 2017). Sample AV1a is, therefore, likely to have accumulated more crystals (or lost more melt) than AF15.

EMP Analyses and SEM Maps

Even though AV1a and AF15 have inherent differences in terms of fabric, bulk compositions, and mineral modes (Table 1 and Figs. 6–7), the plagioclase compositional maps (Figs. 6A.ii–6B.ii) show nearly identical An distributions for the two samples (Fig 6C). The ranges of An contents for the plagioclase show a bell-shaped pattern in both samples with a peak at An_{40-45}. The distributions are similar for most of our sample collection from the Adamello Batholith (Fig. 8) regardless of bulk-rock composition and modal assemblage.

The quantitative EMP data are consistent with those obtained from the SEM phase maps, which show a similar bell-shaped pattern (Fig. 9). To test for disequilibrium among bulk rocks and plagioclase crystals, we show the equilibrium ranges using the $KD_{Ca-Na}^{Min/Liq}$ as used in the statistical analysis of the GEOROC database. We also use recently published experimental data from Adamello Batholith starting compositions to show the range of plagioclase compositions in equilibrium with a rhyolitic melt (<An_{50-55}; Marxer and Ulmer, 2019). As additional visual support, we also display the plagioclase population in disequilibrium from AV1a and AF15 in the modified Rhodes diagram (Fig. 5).
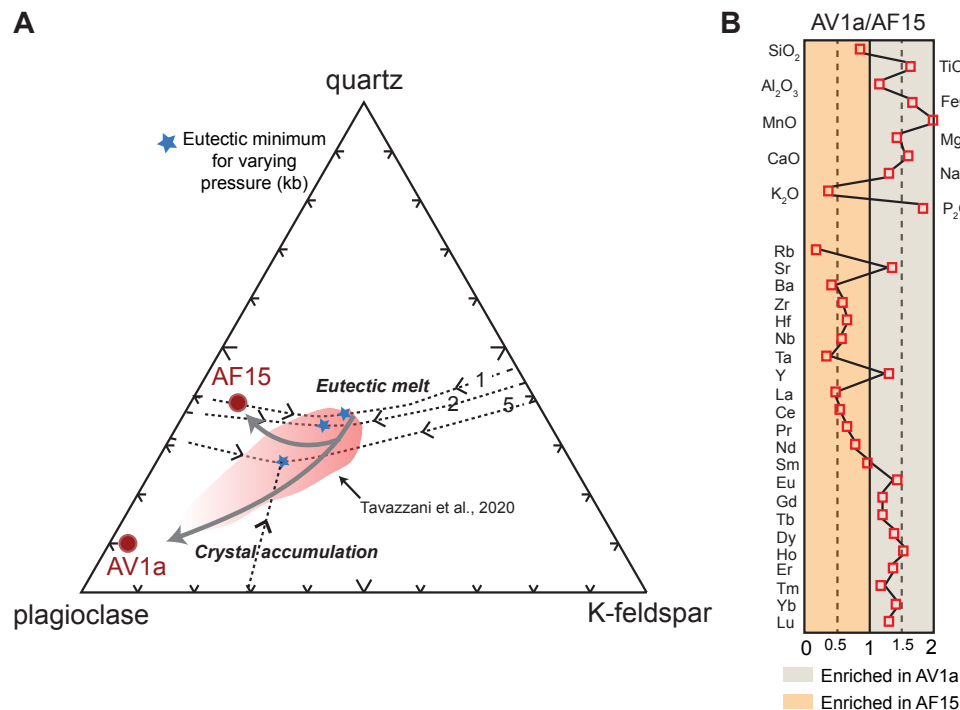
Figure 7. (A) AV1a and AF15 quartz–alkali feldspar–plagioclase modal ratios are projected into a Qz–Or–Ab ternary plot with minimum and eutectic melt at given pressures (kbar). For reference, the range of bulk-rock data from Valle Mosso pluton is plotted (Tavazzani et al., 2020). Grey arrows and blue stars show the trajectories of the minimum melts as a function of increasing pressure, increasing An content, and decreasing aH₂O (Bartoli et al., 2016; Pichavant et al., 2019). (B) Relative enrichment of major and trace elements of AV1a and AF15 where respective elemental contents are ratioed (e.g., AV1a/AF15).
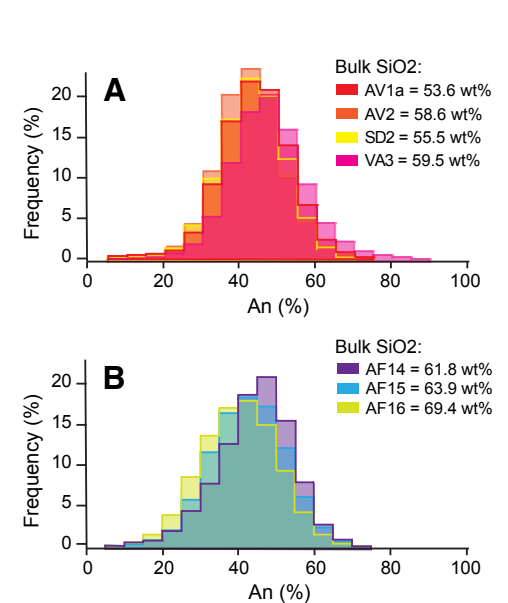
Figure 8. Histograms of anorthite distribution in plagioclase were calculated from plagioclase compositional maps obtained from the workflow described in this paper and the method described in Fiedrich et al. (2017). (A) Re de Castello samples show An distribution in plagioclase for plutonic samples (AV, SD, and VA indicate locality type diorites and tonalites). (B) Western Adamello tonalite samples (WAT) show anorthite distribution in plagioclase for plutonic samples (AF for locality type granodiorites and tonalites).

We observe that in our AV1a plagioclase EMP database (n = 460), ~80% of the plagioclase crystals are in disequilibrium with the bulk rock (Figs. 5 and 9; using the $KD_{Ca-Na}^{Min/liq}$ of 0.27 ± 0.11; Putirka, 2008), including ~70% of the disequilibrium plagioclase compositions being *less An-rich* (more sodic) than the equilibrium range despite the presence of inherited high-An cores. Note that, if we compare the histograms provided by the plagioclase compositional maps (Fig. 6C) with the EMP histogram (Fig. 9), we can see that the high-An cores peak is absent in the plagioclase compositional maps, which suggests that these high-An cores are only a tiny amount of the mapped surface of the thin

section. Thus, the high-An cores signal results from a sampling bias that is not representative of the sample. The latter indicates that using plagioclase compositional maps significantly improves the representation of the dominant plagioclase compositional range in the rock.

In contrast, our AF15 EMP plagioclase database (n = 411) only shows disequilibrium for ~20% of the plagioclase crystals analyzed, which implies crystallization from melts that were closer to the composition of the bulk rock. Due to the chemical evolution of the melt in a closed system (sliding down the "plagioclase loop"), a significant amount of AF15 plagioclase compositions are on the low-An

side of the equilibrium range. This "normal zoning" extends to very low-An compositions (e.g., plagioclase compositional maps with An 5–10, Fig. 8) in AF15 and AV1a, which reflects late stage crystallization from highly evolved rhyolitic trapped melts as the system was reaching its solidus. We note, however, that this low-An plagioclase endmember is very limited in volume.

Thermodynamic Simulations

We compare the observed plagioclase compositions shown in Figs. 6 and 8–9 with calculated
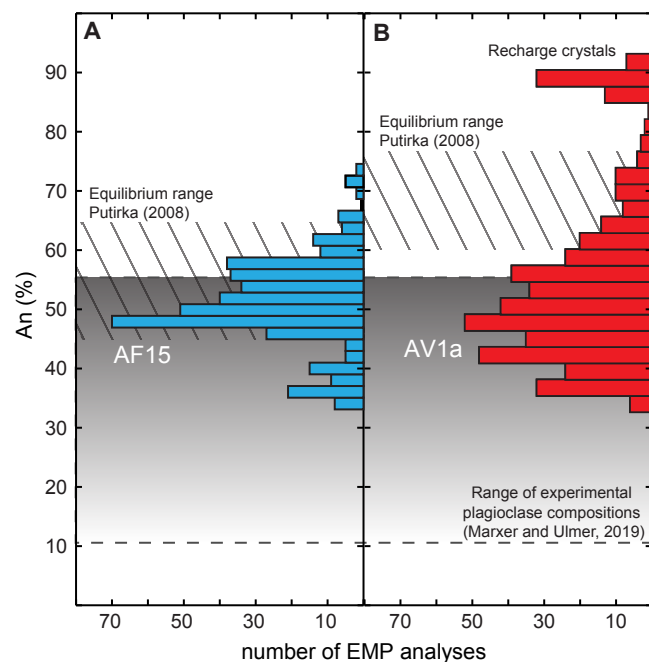
Figure 9. Distribution of plagioclase composition measured with electron microprobe (EMP) is compared with expected equilibrium value of bulk-rock pairs for (A) AF15 and (B) AV1a. We also show the range of composition from experimental data for Adamello Batholith starting compositions (Marxer and Ulmer, 2019). Note the high-An cores in AV1a, which are overrepresented in the electron microprobe (EMP) data (An maps in Figs. 6A.ii–6B.ii show scarce high-An cores).

MatMELTS plagioclase compositions using the starting composition of the samples AF15 and AV1a and the set of conditions listed in Marxer and Ulmer (2019) (cf. Methods Section; Fig. 10). We highlight a subset of simulations that provide an example of our workflow. Other simulations are presented in File S4. Due to known limitations of rhyolite-MELTs to model hornblende stability in water-rich magmas (such as in the Adamello), we use a qualitative rather than a quantitative approach. For example, we expect that the "missing" hornblende may affect plagioclase compositions (e.g., excess Ca, Al, Na, and H_2O in the residual melt). We argue, however, that the thermodynamic simulations can still be useful as a means for identifying silicic cumulates by producing theoretical plagioclase compositional distributions representative of the samples of interest.

In the case of AV1a, significant differences between the simulated (theoretical) and the observed (measured) anorthite distribution in plagioclase can be noted (Fig. 10). Simulated anorthite distributions for AV1a return compositions from An_{85-90} to An_5, but intermediate compositions (An_{30} to An_{60}) are less frequently calculated. Additionally, the range of plagioclase compositions in the AV1a simulations diverges significantly from the equilibrium range predicted by Putirka (2008) and from the experimentally constrained range of compositions (typically An <50; Marxer and Ulmer, 2019). In the case of AF15, "fractionate solids" and "50/50" return fundamentally different simulated anorthite distributions in plagioclase. The "fractionate solids" simulation yields compositions between An_{75} to An_{20} with a low-anorthite compositional peak at An_{20-30}. Thus, the "fractionate solids" simulation failed to accurately reproduce the observed anorthite distribution in plagioclase. However, the "50/50 calculations" do produce a distribution of plagioclase An contents that is similar to those observed in natural samples (Fig. 10). The slight shift observed could be linked to the minor inaccuracies in initial conditions (P, H_2O content, and fO_2) and in the solution models used by

rhyolite-MELTS. The "50/50 simulations" encompass the entire range of compositions calculated via the equilibrium models of Putirka (2008) and the experimentally constrained range of plagioclase compositions of Marxer and Ulmer (2019) (e.g., 92% of predicted An compositions lie within these ranges). The calculated An peak for "50/50 simulations" also coincides with the observed An peak from natural data and the range of An compositions bracketed by the experimental data and the predicted equilibrium values (40 < An < 50).

Melt Depletion in the Adamello Samples

Samples AV1a and AF15 have obvious differences, including a 10 wt% SiO_2 shift in bulk composition, different modes, variation in textures (AV1a is foliated, AF15 is not), and incompatible element enrichment in AF15 relative to AV1a. However, they also display striking similarities, including the same mineral assemblage and the same distribution of plagioclase compositions (e.g., bell-shaped patterns peaking at $\sim An_{40-45}$; Figs. 6C and 8–9). As the plagioclase compositions are dominantly low-An, crystallization must have proceeded from more evolved melt compositions than what is inferred from the AV1a bulk-rock composition, which suggests a significant loss of evolved melt from this sample. Using the AV1a bulk rock as a starting composition for thermodynamic simulations, one observes that the calculated distribution of plagioclase An content is far from the natural distribution. In contrast, the same exercise that uses the AF15 bulk-rock composition as the starting melt composition closely reproduces the observed bell-shaped An distributions in the Adamello plagioclases. These results indicate that AF15 preserved close-to-liquid characteristics while AV1a did not and that both samples were generated from a similar initial bulk magma composition.

■ DISCUSSION AND PERSPECTIVES

The results presented here follow up on recent observations that intermediate to silicic plutonic

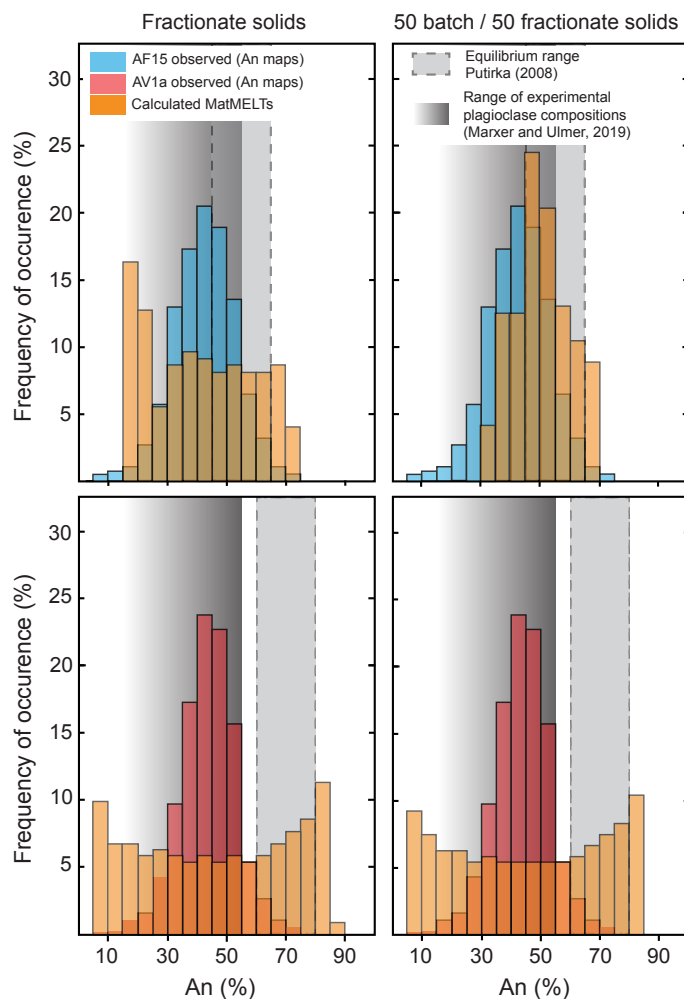Fractionate solids   50 batch / 50 fractionate solids

Figure 10. Histograms plot the frequency of occurrence of calculated versus observed An content in plagioclase of AF15 and AV1a using MatMELTS (calculated) and the plagioclase compositional maps (observed). The simulations use AF15 and AV1a bulk compositions with 6 wt% H$_2$O, a FMQ +1 buffer, and a temperature range from 1100 °C to 700 °C at 2 kbar. The simulations are plotted against the AF15 and AV1a plagioclase equilibrium range from Putirka (2008) and the compositional range for experimental plagioclase (Marxer and Ulmer, 2019).

more evolved than would be expected from their respective bulk rock compositions (plagioclase is less Ca-rich, and mafic minerals are less Mg-rich; Figs. 4–5). Analysis of the global volcanic record, on the other hand, shows a mineral assemblage more in equilibrium with its bulk-rock composition.

Various open-system processes (e.g., recharge/ mixing, assimilation, and melt extraction) or closed-system processes (e.g., melt evolution due to mineral solid solutions) can generate chemical complexities in the mineral assemblages of all igneous rock types. However, we argue that melt extraction at relatively high crystallinity (mush state with > ~50 vol% crystals; Dufek and Bachmann, 2010) is a likely scenario for generating the observed disequilibrium in plutonic rocks. The latter is particularly true when minerals are *significantly more evolved* than their host bulk rocks (Fig. 11). When applying the workflow described in this study to two endmember samples (AV1a and AF15) from the Adamello Batholith, we showed that different amounts of melt loss affected the bulk rock composition of the two samples (Fig. 11). Therefore, we stress that detailed petrological work remains key to estimating how much melt loss (or crystal accumulation) occurred in a given plutonic sample and will also help us better understand the mechanisms associated with melt loss.

Volcanic and plutonic rocks preserve the record of magmatic processes that have shaped our planet through time. Unraveling the information contained in these archives is a fundamental goal of petrology. Using the technique of Ganne et al. (2018), coupled with a comprehensive analytical workflow on natural samples, we show that:

(1) in most cases, plutonic units do not correspond to "quenched melt" compositions but instead represent the cumulates of magma reservoirs.

(2) cumulative signatures are not restricted to mafic or ultramafic compositions but are commonplace in intermediate to silicic plutons such as the Adamello Pluton.

Therefore, determining whether a specific plutonic sample composition embodies a "melt composition" is critical to interpreting its geochemical signature correctly. The amount of melt extraction can be highly variable and needs to be

rocks are partly cumulative (Barnes et al., 2016; Barnes et al., 2020; Bertolett et al., 2019; Fiedrich et al., 2017; Garibaldi et al., 2018; Hartung et al., 2017; Holness, 2018; Keller et al., 2015; Laurent et al., 2020; Lee and Morton, 2015; Tavazzani et al., 2020; Webber et al., 2015; Werts et al., 2020; Wolff, 2017). As most of these studies focused on single plutonic systems, a global assessment of how pervasive melt loss is in plutons worldwide appears

to be an essential step forward. Our investigation into the equilibrium among minerals and bulk-rock pairs in a compiled database (i.e., for plutonic and volcanic rocks) using geochemical tests for mineral-melt equilibria (Rhodes et al., 1979; Putirka, 2008, 2016; Ganne et al., 2018) indicates that most mineral compositions are out of equilibrium with their host bulk-rock compositions (Figs. 2–3). Moreover, minerals in plutonic rocks tend to be chemically

Cornet et al. | Assessing the effect of melt extraction on compositions of granitoids

Figure 11. Sketch shows the different evolutionary paths of two hypothetical (left) A and (right) B magmas. A and B first start from similar conditions (compositions, P, T, and fO_2) and start crystallizing identical crystal populations (e.g., identical plagioclase population as discussed in this article). As the magma reached high crystallinity (probably in the optimal melt extraction window; ~50–70 vol% crystals of Dufek and Bachmann, 2010), variable amounts of extraction occurred. A did not lose as much melt as B, which led to fundamentally different bulk-rock compositions of the final hand samples A(CM) and B(CM) (comparable to AF15 and AV1a, respectively) that can be described as silicic cumulate with different amounts of trapped melt. A(ME) and B(ME) are the extracted melt components that potentially form high-silica granites or other highly differentiated products of magmatism, which are geographically disconnected from their cumulative counterparts, i.e., A(CM) and B(CM). The Harker diagram shows the probable position of each magmatic product according to the hypothetical evolution of an incompatible element in the system (modified from Lee and Morton, 2015).

assessed (e.g., with available methods; Deering and Bachmann, 2010; Gelman et al., 2014, Lee and Morton, 2015; Fiedrich et al., 2018; Werts et al., 2020). We argue that such a step is mandatory to ultimately move toward a deeper understanding of our planet's crustal distillation factory through time.

REFERENCES CITED

Arculus, R.J., and Wills, K.J.A., 1980, The petrology of plutonic blocks and inclusions from the lesser Antilles Island arc: Journal of Petrology, v. 21, no. 4, p. 743–799, https://doi.org/10.1093/petrology/21.4.743.

Bachl, C.A., Miller, C.F., Miller, J.S., and Faulds, J.E., 2001, Construction of a pluton: Evidence from an exposed cross section of the Searchlight pluton, Eldorado Mountains, Nevada: Geological Society of America Bulletin, v. 113, no. 9, p. 1213–1228, https://doi.org/10.1130/0016-7606(2001)113<1213:COAPEF>2.0.CO;2.

Bachmann, O., and Huber, C., 2019, The inner workings of crustal distillation columns; the physical mechanisms and rates controlling phase separation in silicic magma reservoirs: Journal of Petrology, v. 60, p. 3–18, https://doi.org/10.1093/petrology/egy103.

Bacon, C.R., and Druitt, T.H., 1988, Compositional evolution of the zoned calcalkaline magma chamber of Mount Mazama, Crater Lake, Oregon: Contributions to Mineralogy and Petrology, v. 98, no. 2, p. 224–256, https://doi.org/10.1007/BF00402114.

Barnes, C.G., Coint, N., and Yoshinobu, A., 2016, Crystal accumulation in a tilted arc batholith: The American Mineralogist, v. 101, no. 8, p. 1719–1734, https://doi.org/10.2138/am-2016-5404.

Barnes, C.G., Werts, K., Memeti, V., and Ardill, K., 2020, Most granitoid rocks are cumulates: Deductions from hornblende compositions and zircon saturation: Journal of Petrology, v. 60, no. 11, p. 2227–2240, https://doi.org/10.1093/petrology/egaa008.

Bartoli, O., Acosta-Vigil, A., Ferrero, S., and Cesare, B., 2016, Granitoid magmas preserved as melt inclusions in high-grade metamorphic rocks: The American Mineralogist, v. 101, no. 7, p. 1543–1559, https://doi.org/10.2138/am-2016-5541CCBYNCND.

Beane, R., and Wiebe, R.A., 2012, Origin of quartz clusters in Vinalhaven granite and porphyry, coastal Maine: Contributions to Mineralogy and Petrology, v. 163, no. 6, p. 1069–1082, https://doi.org/10.1007/s00410-011-0717-1.

Berger, J., Lo, K., Diot, H., Triantafyllou, A., Plissart, G., and Féménias, O., 2017, Deformation-driven differentiation during in situ crystallization of the 2·7 Ga iguilid mafic intrusion (West African Craton, Mauritania): Journal of Petrology, v. 58, no. 4, p. 819–840, https://doi.org/10.1093/petrology/egx035.

Bertolett, E.M., Prior, D.J., Gravley, D.M., Hampton, S.J., and Kennedy, B.M., 2019, Compacted cumulates revealed by electron backscatter diffraction analysis of plutonic lithics: Geology, v. 47, no. 5, p. 445–448, https://doi.org/10.1130/G45616.1.

Bigazzi, G., Del Moro, A., and Macera, P., 1986, A quantitative approach to trace element and Sr isotope evolution in the Adamello Batholith (northern Italy): Contributions to Mineralogy and Petrology, v. 94, no. 1, p. 46–53, https://doi.org/10.1007/BF00371225.

Bogaerts, M., Scaillet, B., Liégeois, J.P., and Vander Auwera, J., 2003, Petrology and geochemistry of the Lyngdal granodiorite (Southern Norway) and the role of fractional crystallisation in the genesis of Proterozoic ferro-potassic A-type granites: Precambrian Research, v. 124, p. 149–184, https://doi.org/10.1016/S0301-9268(03)00085-8.

Boudreau, A., and Philpotts, A.R., 2002, Quantitative modeling of compaction in the Holyoke flood basalt flow, Hartford Basin, Connecticut: Contributions to Mineralogy and Petrology, v. 144, no. 2, p. 176–184, https://doi.org/10.1007/s00410-002-0391-4.

Chappell, B.W., White, A.J.R., and Hine, R., 1988, Granite provinces and basement terranes in the Lachlan Fold Belt, southeastern Australia: Australian Journal of Earth Sciences, v. 35, no. 4, p. 505–521, https://doi.org/10.1080/08120098808729466.

Connolly, J.A.D., 2009, The geodynamic equation of state: What and how: Geochemistry, Geophysics, Geosystems, v. 10, https://doi.org/10.1029/2009GC002540.

Deering, C.D., and Bachmann, O., 2010, Trace element indicators of crystal accumulation in silicic igneous rocks: Earth and Planetary Science Letters, v. 297, no. 1–2, p. 324–331, https://doi.org/10.1016/j.epsl.2010.06.034.

Duchesne, J.C., Berza, T., Liégeois, J.P., and Vander Auwera, J., 1998, Shoshonitic liquid line of descent from diorite to granite: The Late Precambrian post-collisional Tismana pluton (South Carpathians, Romania): Lithos, v. 45, no. 1–4, p. 281–303, https://doi.org/10.1016/S0024-4937(98)00036-X.

Dufek, J., and Bachmann, O., 2010, Quantum magmatism: Magmatic compositional gaps generated by melt-crystal dynamics: Geology, v. 38, no. 8, p. 687–690, https://doi.org/10.1130/G30831.1.

Fiedrich, A.M., Bachmann, O., Ulmer, P., Deering, C.D., Kunze, K., and Leuthold, J., 2017, Mineralogical, geochemical, and textural indicators of crystal accumulation in the Adamello Batholith (Northern Italy): The American Mineralogist, v. 102, no. 12, p. 2467–2483, https://doi.org/10.2138/am-2017-6026.

Fiedrich, A.M., Martin, L.H.J., Storck, J.C., Ulmer, P., Heinrich, C.A., and Bachmann, O., 2018, The influence of water in silicate melt on aluminium excess in plagioclase as a potential hygrometer: Scientific Reports, v. 8, no. 1, article no. 12421, https://doi.org/10.1038/s41598-018-29178-z.

Frazer, R.E., Coleman, D.S., and Mills, R.D., 2014, Zircon U-Pb geochronology of the Mount Givens Granodiorite: Implications for the genesis of large volumes of eruptible magma: Journal of Geophysical Research: Solid Earth, v. 119, no. 4, p. 2907–2924, https://doi.org/10.1002/2013JB010716.

Frey, F.A., Chappell, B.W., and Roy, S.D., 1978, Fractionation of rare-earth elements in the Tuolumne Intrusive Series, Sierra Nevada batholith, California: Geology, v. 6, no. 4, p. 239–242, https://doi.org/10.1130/0091-7613(1978)6<239:FOREIT>2.0.CO;2.

Ganne, J., Bachmann, O., and Feng, X., 2018, Deep into magma plumbing systems: Interrogating the crystal cargo of volcanic deposits: Geology, v. 46, no. 5, p. 415–418, https://doi.org/10.1130/G39857.1.

Garibaldi, N., Tikoff, B., Schaen, A.J., and Singer, B.S., 2018, Interpreting granitic fabrics in terms of rhyolitic melt segregation, accumulation, and escape via tectonic filter pressing in the Huemul Pluton, Chile: Journal of Geophysical Research: Solid Earth, v. 123, no. 10, p. 8548–8567, https://doi.org/10.1029/2018JB016282.

Gelman, S.E., Deering, C.D., Bachmann, O., Huber, C., and Gutiérrez, F.J., 2014, Identifying the crystal graveyards remaining after large silicic eruptions: Earth and Planetary Science Letters, v. 403, p. 299–306, https://doi.org/10.1016/j.epsl.2014.07.005.

Glazner, A.F., Coleman, D.S., and Mills, R.D., 2018, The volcanic-plutonic connection, in Breitkreuz, C., and Rocchi, S., eds., Advances in Volcanology: Physical Geology of Shallow Magmatic Systems: New York, Springer, p. 61–82, https://doi.org/10.1007/11157_2015_11.

Graeter, K.A., Beane, R.J., Deering, C.D., Gravley, D., and Bachmann, O., 2015, Formation of rhyolite at the Okataina Volcanic Complex, New Zealand: New insights from analysis of quartz clusters in plutonic lithics: The American Mineralogist, v. 100, p. 1778–1789, https://doi.org/10.2138/am-2015-5135.

Gualda, G.A.R., Ghiorso, M.S., Lemons, R.V., and Carley, T.L., 2012, Rhyolite-MELTS: A modified calibration of MELTS optimized for silica-rich, fluid-bearing magmatic systems: Journal of Petrology, v. 53, no. 5, p. 875–890, https://doi.org/10.1093/petrology/egr080.

Hansmann, W., and Oberli, F., 1991, Zircon inheritance in an igneous rock suite from the southern Adamello batholith (Italian Alps)—Implications for petrogenesis: Contributions to Mineralogy and Petrology, v. 107, no. 4, p. 501–518, https://doi.org/10.1007/BF00310684.

Hartung, E., Caricchi, L., Floess, D., Wallis, S., Harayama, S., Kouzmanov, K., and Chiaradia, M., 2017, Evidence for residual melt extraction in the Takidani Pluton, Central Japan: Journal of Petrology, v. 58, no. 4, p. 763–788, https://doi.org/10.1093/petrology/egx033.

Holness, M.B., 2018, Melt segregation from silicic crystal mushes: A critical appraisal of possible mechanisms and their microstructural record: Contributions to Mineralogy and Petrology, v. 173, no. 6, p. 48, https://doi.org/10.1007/s00410-018-1465-2.

Hoskin, P.W.O., Kinny, P.D., Wyborn, D., and Chappell, B.W., 2000, Identifying accessory mineral saturation during differentiation in granitoid magmas: An integrated approach: Journal of Petrology, v. 41, no. 9, p. 1365–1396, https://doi.org/10.1093/petrology/41.9.1365.

Jagoutz, O., and Schmidt, M.W., 2012, The formation and bulk composition of modern juvenile continental crust: The Kohistan arc: Chemical Geology, v. 298–299, p. 79–96, https://doi.org/10.1016/j.chemgeo.2011.10.022.

Johannes, W., and Holtz, F., 1996, The haplogranite system Qz-Ab-Or, in Petrogenesis and Experimental Petrology of Granitic Rocks: Berlin, Heidelberg, Germany, Springer, p. 18–57, https://doi.org/10.1007/978-3-642-61049-3_2.

Kagami, H., Ulmer, P., Hansmann, W., Dietrich, V., and Steiger, R.H., 1991, Nd-Sr isotopic and geochemical characteristics of the southern Adamello (northern Italy) intrusives: Implications for crustal versus mantle origin: Journal of Geophysical Research: Solid Earth, v. 96, p. 14331–14346, https://doi.org/10.1029/91JB01197.

Keller, C.B., Schoene, B., Barboni, M., Samperton, K.M., and Husson, J.M., 2015, Volcanic-plutonic parity and the differentiation of the continental crust: Nature, v. 523, no. 7560, p. 301–307, https://doi.org/10.1038/nature14584.

Laurent, O., Björnsen, J., Wotzlaw, J., Bretscher, S., Pimenta Silva, M., Moyen, J.F., Ulmer, P., and Bachmann, O., 2020, Earth's earliest granitoids are crystal-rich magma reservoirs tapped by silicic eruptions: Nature Geoscience, v. 13, no. 2, p. 163–169, https://doi.org/10.1038/s41561-019-0520-6.

Lee, C.T.A., and Morton, D.M., 2015, High silica granites: Terminal porosity and crystal settling in shallow magma chambers: Earth and Planetary Science Letters, v. 409, p. 23–31, https://doi.org/10.1016/j.epsl.2014.10.040.

Lewis, J.F., 1973, Petrology of the ejected plutonic blocks of the soufrière volcano, St. Vincent, west Indies: Journal of Petrology, v. 14, no. 1, p. 81–112, https://doi.org/10.1093/petrology/14.1.81.

Liebske, C., 2015, ISpectra: An open source toolbox for the analysis of spectral images recorded on scanning electron microscopes: Microscopy and Microanalysis, v. 21, no. 4, p. 1006–1016, https://doi.org/10.1017/S1431927615014336.

Marxer, F., and Ulmer, P., 2019, Crystallisation and zircon saturation of calc-alkaline tonalite from the Adamello Batholith at upper crustal conditions: An experimental study: Contributions to Mineralogy and Petrology, v. 174, no. 10, p. 1–29, https://doi.org/10.1007/s00410-019-1619-x.

Memeti, V., Paterson, S., Matzel, J., Mundil, R., and Okaya, D., 2010, Magmatic lobes as "snapshots" of magma chamber growth and evolution in large, composite batholiths: An example from the Tuolumne intrusion, Sierra Nevada, California: Geological Society of America Bulletin, v. 122, no. 11–12, p. 1912–1931, https://doi.org/10.1130/B30004.1.

Meurer, W.P., and Boudreau, A.E., 1996, Compaction of density-stratified cumulates: Effect on trapped-liquid distribution: The Journal of Geology, v. 104, no. 1, p. 115–120, https://doi.org/10.1086/629805.

Miller, C.F., McDowell, S.M., and Mapes, R.W., 2003, Hot and cold granites: Implications of zircon saturation temperatures and preservation of inheritance: Geology, v. 31, no. 6, p. 529–532, https://doi.org/10.1130/0091-7613(2003)031<0529:HACGIO>2.0.CO;2.

Moyen, J.F., Martin, H., and Jayananda, M., 2001, Multi-element geochemical modelling of crust-mantle interactions during late-Archaean crustal growth: The Closepet granite (South India): Precambrian Research, v. 112, no. 1–2, p. 87–105, https://doi.org/10.1016/S0301-9268(01)00171-1.

Pennacchioni, G., Di Toro, G., Brack, P., Menegon, L., and Villa, I.M., 2006, Brittle-ductile-brittle deformation during cooling of tonalite (Adamello, Southern Italian Alps): Tectonophysics, v. 427, no. 1–4, p. 171–197, https://doi.org/10.1016/j.tecto.2006.05.019.

Perfit, M.R., Gust, D.A., Bence, A.E., Arculus, R.J., and Taylor, S.R., 1980, Chemical characteristics of island-arc basalts: Implications for mantle sources: Chemical Geology, v. 30, no. 3, p. 227–256, https://doi.org/10.1016/0009-2541(80)90107-2.

Pichavant, M., Weber, C., and Villaros, A., 2019, Effect of anorthite on granite phase relations: Experimental data and models: Comptes Rendus Geoscience, v. 351, no. 8, p. 540–550, https://doi.org/10.1016/j.crte.2019.10.001.

Putirka, K., 2016, Special collection: Rates and depths of magma ascent on earth: Amphibole thermometers and barometers for igneous systems and some implications for eruption mechanisms of felsic magmas at arc volcanoes: The American Mineralogist, v. 101, no. 4, p. 841–858, https://doi.org/10.2138/am-2016-5506.

Putirka, K.D., 2008, Thermometers and barometers for volcanic systems: Reviews in Mineralogy and Geochemistry, v. 69, no. 1, p. 61–120, https://doi.org/10.2138/rmg.2008.69.3.

Putirka, K.D., 2017, Down the crater: Where magmas are stored and why they erupt: Elements, v. 13, no. 1, p. 11–16, https://doi.org/10.2113/gselements.13.1.11.

Putirka, K.D., Canchola, J., Rash, J., Smith, O., Torrez, G., Paterson, S.R., and Ducea, M.N., 2014, Pluton assembly and the genesis of granitic magmas: Insights from the GIC pluton in cross section, Sierra Nevada Batholith, California: The American Mineralogist, v. 99, no. 7, p. 1284–1303, https://doi.org/10.2138/am.2014.4564.

Rhodes, J.M., Dungan, M.A., Blanchard, D.P., and Long, P.E., 1979, Magma mixing at mid-ocean ridges: Evidence from basalts drilled near 22° N on the Mid-Atlantic Ridge: Tectonophysics, v. 55, no. 1–2, p. 35–61, https://doi.org/10.1016/0040-1951(79)90334-2.

Schaltegger, U., Brack, P., Ovtcharova, M., Peytcheva, I., Schoene, B., Stracke, A., Marocchi, M., and Bargossi, G.M., 2009, Zircon and titanite recording 1.5 million years of magma accretion, crystallization and initial cooling in a composite pluton (southern Adamello Batholith, northern Italy): Earth and Planetary Science Letters, v. 286, no. 1–2, p. 208–218, https://doi.org/10.1016/j.epsl.2009.06.028.

Schoene, B., Schaltegger, U., Brack, P., Latkoczy, C., Stracke, A., and Günther, D., 2012, Rates of magma differentiation and emplacement in a ballooning pluton recorded by U-Pb TIMS-TEA, Adamello Batholith, Italy: Earth and Planetary Science Letters, v. 355–356, p. 162–173, https://doi.org/10.1016/j.epsl.2012.08.019.

Shirley, D.N., 1986, Compaction of igneous cumulates: The Journal of Geology, v. 94, no. 6, p. 795–809, https://doi.org/10.1086/629088.

Stephens, W.E., Whitley, J.E., Thirlwall, M.F., and Halliday, A.N., 1985, The Criffell zoned pluton: Correlated behaviour of rare earth element abundances with isotopic systems: Contributions to Mineralogy and Petrology, v. 89, no. 2–3, p. 226–238, https://doi.org/10.1007/BF00379456.

Tappa, M.J., Coleman, D.S., Mills, R.D., and Samperton, K.M., 2011, The plutonic record of a silicic ignimbrite from the Latir volcanic field, New Mexico: Geochemistry, Geophysics, Geosystems, v. 12, https://doi.org/10.1029/2011GC003700.

Tavazzani, L., Peres, S., Sinigoi, S., Demarchi, G., Economos, R.C., and Quick, J.E., 2020, Timescales and mechanisms of crystal-mush rejuvenation and melt extraction recorded in Permian plutonic and volcanic rocks of the Sesia Magmatic System (southern Alps, Italy): Journal of Petrology, v. 61, no. 5, p. 49, https://doi.org/10.1093/petrology/egaa049.

Taylor, S.R., 1989, Growth of planetary crusts: Tectonophysics, v. 161, no. 3–4, p. 147–156, https://doi.org/10.1016/0040-1951(89)90151-0.

Tuttle, O.F., and Bowen, N.L., 1958, Origin of Granite in the Light of Experimental Studies in the System $NaAlSi_3O_8$–$KAlSi_3O_8$–SiO_2–H_2O: Geological Society of America Memoir 74, 145 p., https://doi.org/10.1130/MEM74-p1.

Vigneresse, J.L., Barbey, P., and Cuney, M., 1996, Rheological transitions during partial melting and crystallization with application to felsic magma segregation and transfer: Journal of Petrology, v. 37, no. 6, p. 1579–1600, https://doi.org/10.1093/petrology/37.6.1579.

Wager, L.R., 1962, Igneous cumulates from the 1902 eruption of Soufrière, St. Vincent: Bulletin Volcanologique, v. 24, no. 1, p. 93–99, https://doi.org/10.1007/BF02599333.

Wager, L.R., Brown, G.M., and Wadsworth, W.J., 1960, Types of igneous cumulates: Journal of Petrology, v. 1, no. 1, p. 73–85, https://doi.org/10.1093/petrology/1.1.73.

Walker, B.A., Bergantz, G.W., Otamendi, J.E., Ducea, M.N., and Cristofolini, E.A., 2015, A MASH zone revealed: The mafic complex of the Sierra Valle Fértil: Journal of Petrology, v. 56, no. 9, p. 1863–1896, https://doi.org/10.1093/petrology/egv057.

Waters, L.E., and Lange, R.A., 2015, An updated calibration of the plagioclase-liquid hygrometer-thermometer applicable to basalts through rhyolites: The American Mineralogist, v. 100, no. 10, p. 2172–2184, https://doi.org/10.2138/am-2015-5232.

Webber, J.R., Klepeis, K.A., Webb, L.E., Cembrano, J., Morata, D., Mora-Klepeis, G., and Arancibia, G., 2015, Deformation and magma transport in a crystallizing plutonic complex, Coastal Batholith, central Chile: Geosphere, v. 11, no. 5, p. 1401–1426, https://doi.org/10.1130/GES01107.1.

Werts, K., Barnes, C.G., Memeti, V., Ratschbacher, B., Williams, D., and Paterson, S.R., 2020, Hornblende as a tool for assessing mineral-melt equilibrium and recognition of crystal accumulation: The American Mineralogist, v. 105, no. 1, p. 77–91, https://doi.org/10.2138/am-2020-6972.

Wiebe, R.A., and Collins, W.J., 1998, Depositional features and stratigraphic sections in granitic plutons: Implications for the emplacement and crystallization of granitic magma: Journal of Structural Geology, v. 20, no. 9–10, p. 1273–1289, https://doi.org/10.1016/S0191-8141(98)00059-5.

Wolff, J.A., 2017, On the syenite-trachyte problem: Geology, v. 45, no. 12, p. 1067–1070, https://doi.org/10.1130/G39415.1.

Wyborn, D., Chappell, B.W., and James, M., 2001, Examples of convective fractionation in high-temperature granites from the Lachlan Fold Belt: Australian Journal of Earth Sciences, v. 48, no. 4, p. 531–541, https://doi.org/10.1046/j.1440-0952.2001.00877.x.